ACS Energy LETTERS

http://pubs.acs.org/journal/aelccp

LETTER

A Hexacyanomanganate Negolyte for Aqueous Redox Flow Batteries

Ji-Eun Jang, S. Jayasubramaniyan, Seok Woo Lee, and Hyun-Wook Lee*

Cite This: *ACS Energy Lett.* 2023, 8, 3702−3709

Read Online

ACCESS | Metrics & More | Article Recommendations | Supporting Information

ABSTRACT: Aqueous redox flow batteries (RFBs) have emerged as promising large-scale energy storage devices due to their high scalability, safety, and flexibility. Manganese-based redox materials are promising sources for use in RFBs owing to their earth abundance, affordability, and variety of oxidation states. However, the instability of Mn redox couples, attributed to the unstable d-orbital configuration of $Mn^{3+}(d^4)$ known to involve strong Jahn−Teller effects, has hindered their practical use. Here, we discover that the $[Mn(CN)_6]^{5-/4-/3-}$ negolyte offers advantages in terms of reversibility, stability, and reaction kinetics owing to the addition of NaCN supporting electrolyte, which inhibits ligand exchange reactions, resulting in high performance. $[Mn(CN)_6]^{5-/4-/3-}$ negolyte possesses stable multielectron reactions from Mn(I) to Mn(III), leading to a high capacity of 133.7 mAh after 100 cycles. We provide chemical evidence obtained from *in situ* Raman analysis for unprecedented Mn(I) stability during electrochemical cycling, opening up new avenues for the design of low-cost Mn-based redox systems.

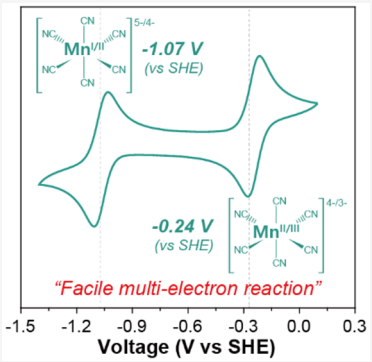

As the world becomes increasingly concerned about the global climate crisis and the imperative transition to a carbon-neutral society, renewable energy sources such as solar and wind power are attracting increasing public concerns.[1,2] However, the intermittent energy produced by renewable sources has highlighted the need for energy storage systems (ESSs) that are efficient and provide long-term stability.[3] Although conventional lithium-ion batteries are well-recognized as a pioneering technology for battery-based ESSs, their high manufacturing costs and safety issues arising from flammable electrolytes limit their use in large-scale ESSs.[4,5] Aqueous redox flow batteries (RFBs) have emerged as a promising technology for large-scale and long-duration energy storage owing to their durability and scalability. They can also decouple energy and power densities, which reduces the levelized cost of energy for operations on a MWh scale.[6−8] Since the first RFBs were developed in the 1970s by NASA in the United States using iron−chromium compounds,[9] diverse redox chemistries have been proposed, including all-vanadium,[10] zinc-based,[11−14] and more recently, metal-complex or water-soluble organic materials.[15−19] Among them, all-vanadium RFBs are the most established and closest to commercialization; however, the price volatility of vanadium resources and their relatively low energy density (25−35 Wh L^{-1}) have posed significant obstacles to the widespread market adoption of ESSs.[5,20] Consequently, researchers continue to improve extant RFB systems and investigate new redox couples.[21,22]

Manganese-based redox materials are promising sources for use in RFBs due to their earth abundance, affordability, and variety of oxidation states.[23] Among Mn redox couples, the $Mn^{2+}(aq)/Mn^{3+}(aq)$ redox couple has been extensively studied as a potential material for various flow battery systems, such as Zn-Mn and Fe-Mn flow batteries,[24,25] owing to its high solubility and high reduction potential (1.51 V vs SHE). However, the use of Mn^{3+} is problematic, as it involves well-known strong Jahn−Teller effects and the Mn^{3+} undergoes a disproportionation reaction in which Mn^{3+} ions transform into $Mn^{IV}O_2(s)$ and Mn^{2+} ions due to the less stable d-orbital configuration of $Mn^{3+}(d^4)$, leading to instability and capacity degradation of the battery system.[26,27] To address this challenge, alternative strategies involving $Mn^{2+}(aq)/Mn^{IV}O_2(s)$ multielectron reactions (1.23 V vs SHE) have been implemented. For instance, Cui et al. proposed an aqueous-based manganese−hydrogen battery employing this $Mn^{2+}(aq)/Mn^{IV}O_2(s)$ redox reaction,[28] resulting in an increase in theoretical capacity due to the two-electron reaction. This strategy has been adopted in several RFB systems, as evidenced by earlier reports.[29−31] Although this two-electron reaction has been controversial due to the presence of an unstable Mn^{3+}

Received: June 28, 2023
Accepted: August 2, 2023
Published: August 8, 2023

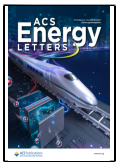

intermediate state, the complexation effect from acetate (CH_3COO^-) ligands allowed for the bypass of the unstable Mn^{3+} state during the $Mn^{2+}(aq)/Mn^{IV}O_2(s)$ reaction, demonstrating the strategic role of ligand selection in overcoming inherent reaction challenges.[32−34] $Mn^0(s)/Mn^{II}(aq)$ reactions, which are generated by the deposition of zerovalent manganese, have been considered as anode redox reactions in RFBs. Schmucker et al. presented $Mn^0/[Mn^{II}Cl_4]^{2-}$ redox materials (−1.18 V vs SHE) consisting of an all-manganese-based flow battery coupled with $[Mn^{II}Cl_4]^{2-}/[Mn^{III}Cl_5]^{2-}$.[35] However, solid/liquid redox reactions involving $Mn^0(s)$ and $Mn^{IV}(s)$ states tend to be complicated because of the presence of intermediate steps, resulting in slow kinetics and poor capacity reversibility due to nonuniform coverage of solid Mn or MnO_2 layers on the electrode.[36,37] Therefore, the development of effective and stable Mn-based redox materials for RFBs remains an important research area.

To attain stability in all-solution-based redox reactions, researchers have investigated a strategy for stabilizing Mn ions using extremely acidic conditions or metal-ion additives such as Ti^{4+} or V^{5+}.[38,39] Using knowledge of the coordination chemistry is a common technique for modifying the properties of metal ions. The complexation effect that occurs during the formation of metal−ligand complexes is known to stabilize the central metal ion.[40,41] Recently, Yu et al. effectively enhanced the cycle life of a Zn-$Mn^{2+/3+}$ flow battery by introducing EDTA ligands to Mn ions and achieving a stable Mn(II)/Mn(III) redox reaction in an aqueous solution.[42] Another group, led by Sleightholme et al., has proposed a new prototype single-material flow battery system that employs acetylacetone (acac) ligands in a nonaqueous system to enable the use of Mn(II), Mn(IV), and Mn(V) oxidation states as negolyte and posolyte materials. The resulting $[Mn^{II}(acac)_3]^-/Mn^{III}(acac)_3$ (−0.4 V vs Ag/Ag^+) and $[Mn^{III/IV}(acac)_3]^+$ (0.7 V vs Ag/Ag^+) redox couples showed a thermodynamic full-cell voltage of 1.1 V.[43]

Similarly, using cyanide ligands can provide opportunities to operate Mn ions in various oxidation states including stable Mn(III) complexes. The octahedral hexacyanomanganate ($Mn(CN)_6$) has been reported to possess Mn(0), Mn(I), Mn(II), Mn(III), and Mn(IV) oxidation states that bond with cyanide ligands.[44] The presence of cyanide ligands induces a low-spin state of the Mn d-orbital, rendering the Mn(III) state relatively more stable and mitigating the inherent problem of Mn(III) disproportionation observed in the previous research.[44,45] In particular, the presence of cyanide ligands facilitates the formation of a stable complex containing the Mn(I) state, which is generally rare. The t_{2g} set of d-orbitals in $[Mn^{I}(CN)_6]^{5-}$ is completely occupied with 6 electrons at the Mn(I) state, which is an electron configuration similar to that of $[Fe^{II}(CN)_6]^{4-}$ or $[Co^{III}(CN)_6]^{3-}$.[46] $Mn(CN)_6$ has demonstrated promise as a candidate for negolyte materials in aqueous RFBs, which are typically challenging to find due to the difficulties associated with sluggish redox kinetics and parasitic hydrogen evolution reactions.[47−49] The $[Mn^{I}(CN)_6]^{5-}/[Mn^{II}(CN)_6]^{4-}$ and $[Mn^{II}(CN)_6]^{4-}/[Mn^{III}(CN)_6]^{3-}$ redox couples possess proper reduction potentials of −1.1 and −0.24 V vs SHE, respectively, in aqueous solutions (Figure 1a).[44,50−52] The weak Jahn−Teller distortion that arises from the low-spin nature of d-electron configurations in Mn enables facile redox reactions of the $Mn(CN)_6$ complex, similar to the case of the hexacyanochromate redox couple ($[Cr(CN)_6]^{4-/3-}$) as a negolyte material,

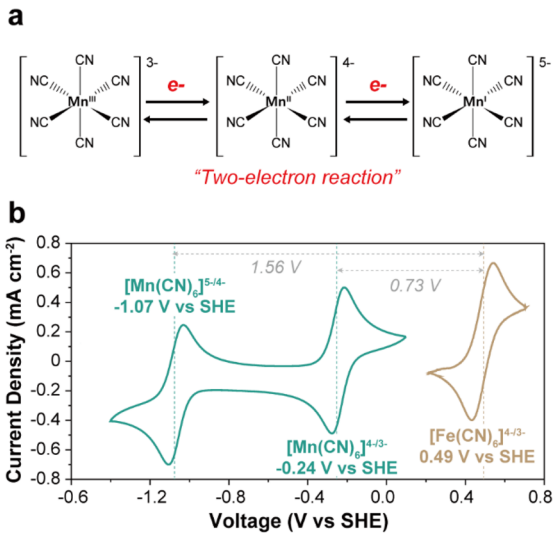

Figure 1. Concept of $Mn(CN)_6$-based flow cell. (a) Scheme of the multielectron reaction of hexacyanomanganate ions. (b) Cyclic voltammograms (CVs) of $[Mn(CN)_6]^{5-/4-/3-}$ (blue) and $[Fe(CN)_6]^{4-/3-}$ (brown) redox couples at a scan rate of 20 mV s^{-1}, which were used as the negolyte and posolyte, respectively.

which was previously introduced by our group.[22] However, there has been no prior investigation of the potential of $Mn(CN)_6$ redox materials in RFBs, specifically the liquid-based Mn(I)/Mn(II) redox reaction in rechargeable battery systems. The solid/solid reaction utilizing the oxidation states of Mn(I) to Mn(III) has been proposed as cathode materials for sodium-ion rechargeable batteries in the form of manganese hexacyanomanganate ($Na_xMn[Mn(CN)_6]$, where x ranges from 0 to 3).[53−55]

To this end, we demonstrate the successful implementation of a practical RFB system that uses hexacyanomanganate ions as a negolyte. Our investigation revealed that the $Mn(CN)_6$ ions undergo labile redox reactions from Mn(I) to Mn(III) without severe parasitic hydrogen evolution reactions when added by a sodium cyanide (NaCN) supporting electrolyte. To validate the feasibility of the system, we configured a full cell using a $Mn(CN)_6$ negolyte coupled with a hexacyanoferrate ($[Fe(CN)_6]^{4-/3-}$) posolyte, as illustrated in Figure 1b. Throughout the cell operation, we monitored the CN stretching modes of Mn using *in situ* Raman spectroscopy. Our results validated that the oxidation state of Mn effectively changes during the charge and discharge processes. To the best of our knowledge, this is the first demonstration of the Mn(I)/Mn(II) redox reaction in an aqueous RFB system, which represents a significant advance in the development of redox materials for aqueous RFBs.

Kinetic Properties of $[Mn^{I}(CN)_6]^{5-}/[Mn^{II}(CN)_6]^{4-}$ and $[Mn^{II}(CN)_6]^{4-}/[Mn^{III}(CN)_6]^{3-}$ Redox Couples. The $Mn(CN)_6$ negolyte used in this study was sourced from as-synthesized $K_3[Mn(CN)_6]$ and characterized using X-ray diffraction (XRD) and UV−vis spectroscopy (see Supplementary Figures 1 and 2). The redox properties of the $[Mn(CN)_6]^{5-/4-/3-}$ anions were investigated through cyclic voltammetry (CV) testing. During the electrochemical experiments, a cyanide-rich supporting electrolyte was used to mitigate the rapid hydrolysis reaction that occurs in the absence of excessive cyanide ligands, which results in the formation of manganese hydroxide ($Mn(OH)_x$) or manganese

https://doi.org/10.1021/acsenergylett.3c01293
ACS Energy Lett. 2023, 8, 3702−3709

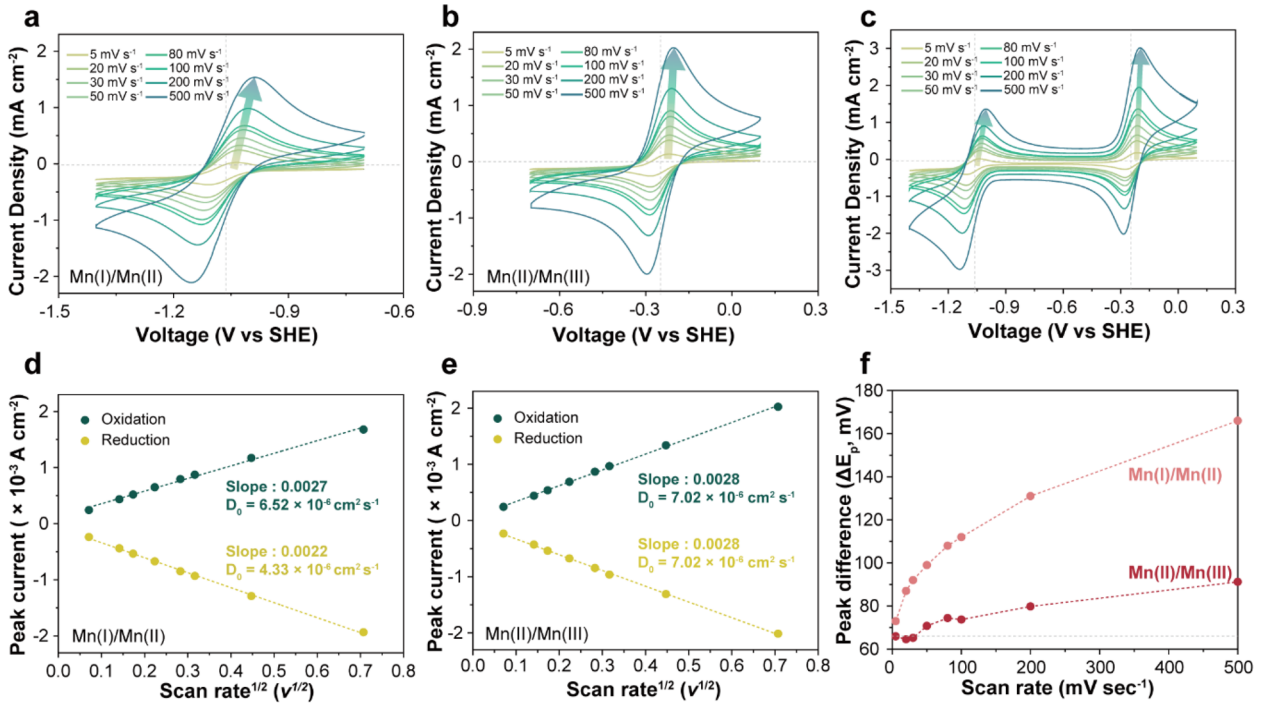

Figure 2. Electrochemical behavior of hexacyanomanganate redox couples ($[Mn(CN)_6]^{5-/4-/3-}$). CVs of 5 mM $K_3[Mn(CN)_6]$ negolyte with 3 M NaCN supporting electrolyte at various scan rates (5, 20, 30, 50, 80, 100, 200, and 500 mV s^{-1}): (a) $[Mn^{I/II}(CN)_6]^{5-/4-}$ and (b) $[Mn^{II/III}(CN)_6]^{4-/3-}$ redox reactions. (c) CVs of the entire voltage range containing all redox reactions. (d, e) Linear relationship between $(\text{scan rate})^{1/2}$ and peak current density corresponding to (a) (d) and (b) (e). (f) Peak difference at various scan rates of Mn(I)/Mn(II) and Mn(II)/Mn(III), which correspond to (a) and (b), respectively.

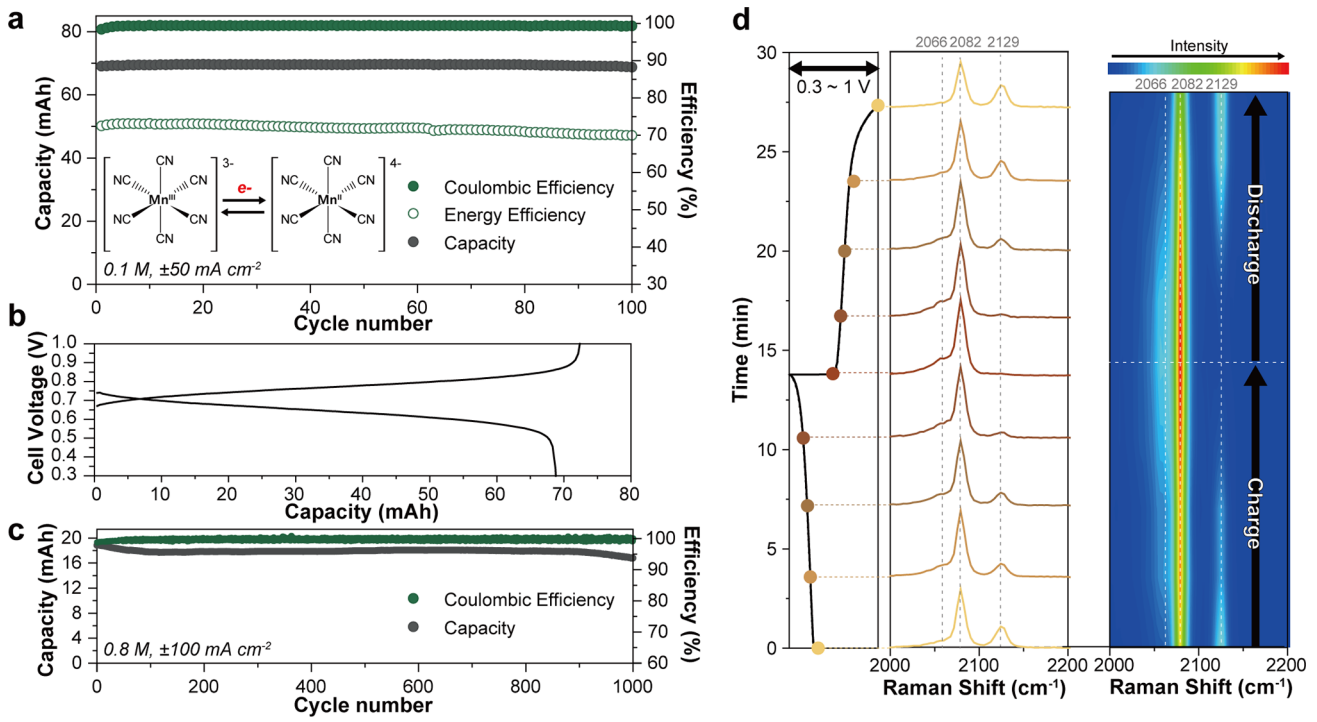

Figure 3. Analysis of full-cell performance for $K_3[Mn(CN)_6]$ negolyte at 0.1 and 0.4 M concentrations (one-electron reaction). (a) Coulombic efficiency, energy efficiency, and capacity of 0.1 M $K_3[Mn(CN)_6]$ full-cells for 100 cycles. (b) The typical galvanostatic charging−discharging plots, corresponding to (a). (c) Coulombic efficiency and capacity of the full-cell constructed with 0.8 M negolyte for 1000 cycles. (d) *In situ* Raman spectra of 0.1 M $K_3[Mn(CN)_6]$ negolyte during full-cell operation. The left panel indicates the CN-stretches of the negolyte at each charging state, and the right panel shows the intensity of the CN-stretches during a single cycle (charge and discharge). The full cell test with 0.1 M negolyte was conducted at ±50 mA cm^{-2} in the voltage range of 0.3−1 V. The 0.8 M cell was operated at ±100 mA cm^{-2} within the voltage range of 0.2−1.1 V.

https://doi.org/10.1021/acsenergylett.3c01293
ACS Energy Lett. 2023, 8, 3702−3709

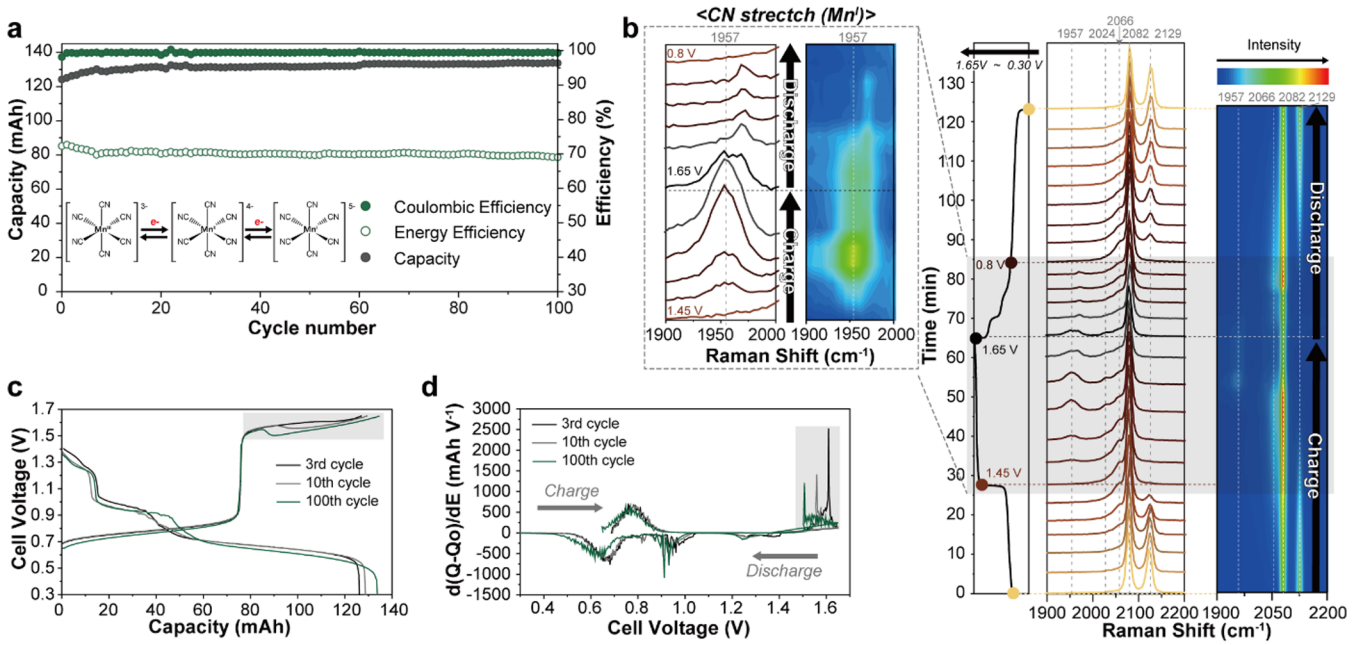

Figure 4. Analysis of full-cell performance for $K_3[Mn(CN)_6]$ negolyte using the two-electron reaction. (a) Plots of the Coulombic efficiency, energy efficiency, and capacity during 100 cycles. (b) *In situ* Raman spectra of 0.1 M $K_3[Mn(CN)_6]$ negolyte during a single cycle (charge and discharge). The line spectra indicate the CN stretching of $Mn(CN)_6$ at different SOCs, and the contour graphs display the relative intensity of the line spectra. The left panel (dotted box) presents magnified Raman spectra of the Mn(I)/Mn(II) redox region (gray mark of the right panel), which indicates CN^- stretches of $[Mn^I(CN)_6]^{5-}$. (c) Galvanostatic charging−discharging plots of two-electrons reaction at the 3rd, 10th, and 100th cycles. (d) dq/dV plots corresponding to (c). The cells during *in situ* testing and cycle testing were operated at ±30 mA cm^{-2} in the range of 1.0−1.65 V.

oxide (MnO_x).[45] This approach has been previously employed for hexacyanochromate ions ($[Cr(CN)_6]^{4-/3-}$) with the addition of a sodium cyanide (NaCN) supporting electrolyte, successfully suppressing the hydrolysis of $[Cr(CN)_6]^{4-/3-}$ ions and hydrogen evolution reactions.[22] This strategy led to the development of a flow battery system with decent performance and high electrochemical stability. CV plots were obtained at various scan rates (5−500 mV s^{-1}) according to different voltage ranges to fulfill the desired redox-species-dependent redox reactions. The oxidation states of Mn in hexacyanomanganate ions can vary between +1 and +3. As shown in Figure 2a−c, the CV diagrams derived for both $[Mn^I(CN)_6]^{5-}/[Mn^{II}(CN)_6]^{4-}$ (at −1.07 V vs SHE) and $[Mn^{II}(CN)_6]^{4-}/[Mn^{III}(CN)_6]^{3-}$ (at −0.24 V vs SHE) redox reactions exhibit distinct duck-shaped curves, indicating stable and facile redox reactions. Figure 2d,e indicates that the redox reactions are governed by a diffusion-limited system according to the linear relationship between $(\text{scan rate})^{1/2}$ and peak current density. The diffusion coefficients (D_0) for each reaction were calculated from the Randles−Sevcik equation, implying the fast electrochemical kinetics of the two redox reactions. Figure 2f and Supplementary Table 1 provide the peak differences (ΔE_p) of each redox reaction, as shown in Figure 2a,b. The $[Mn^I(CN)_6]^{5-}/[Mn^{II}(CN)_6]^{4-}$ redox reaction has a ΔE_p range of 61.9−85.4 mV for scan rates of 5−500 mV s^{-1}, whereas the $[Mn^{II}(CN)_6]^{4-}/[Mn^{III}(CN)_6]^{3-}$ redox reaction has a range of 68−140 mV. In particular, the $[Mn^{II}(CN)_6]^{4-}/[Mn^{III}(CN)_6]^{3-}$ reaction exhibits nearly reversible behavior at scan rates of 5−50 mV s^{-1}, with a peak difference in the range of 61.9−66 mV. This peak difference is close to the theoretical value (60 mV) predicted for an ideal one-electron reversible reaction. The charge transfer rate (k_0) of the redox reactions was also calculated using the Nicholson method,[56] with calculated k_0 values of 3.44×10^{-3} and 1.78×10^{-2} cm s^{-1} for the $[Mn^I(CN)_6]^{5-}/[Mn^{II}(CN)_6]^{4-}$ and $[Mn^{II}(CN)_6]^{4-}/[Mn^{III}(CN)_6]^{3-}$ reactions, respectively, indicating that both redox reactions exhibit quasi-reversible behaviors. The obtained D_0 and k_0 of $Mn(CN)_6$ redox reactions are summarized in Supplementary Table 2. The fundamental electrochemical analysis reveals that the $[Mn(CN)_6]^{5-/4-/3-}$ complexes have a labile two-electron redox reaction with an appropriate standard reduction potential, thereby providing a potential negolyte for the RFB systems.

$[Mn(CN)_6]^{5-/4-/3-}$-Based Flow Cell Operation. *One-Electron Reaction.* Based on the electrochemical properties of $[Mn(CN)_6]^{5-/4-/3-}$ redox couples, the redox potentials of $[Mn(CN)_6]^{5-/4-/3-}$ and $[Fe(CN)_6]^{4-/3-}$ are 0.73 and 1.56 V, respectively, as shown in Figure 1a. Two distinct galvanostatic charging−discharging tests were performed: one using only the $[Mn(CN)_6]^{4-/3-}$ redox couple (one-electron reaction), and the other using both the $[Mn(CN)_6]^{4-/3-}$ and $[Mn(CN)_6]^{5-/4-}$ redox couples (two-electron reaction) by adjusting the charging cutoff voltage. The full-cell performance was investigated employing $[Mn(CN)_6]^{4-/3-}$ redox couples with 0.1 and 0.4 M concentrations of negolytes over a voltage range of 0.3−1.0 V, as shown in Figure 3a and Supplementary Figures 3 and 4. The flow cell exhibited a high average Coulombic efficiency (CE) of 99.36% and an energy efficiency (EE) of 71.84% after 100 cycles for 56.3 h (see also Supplementary Figure 3b). Supplementary Figure 4 shows the typical galvanostatic profiles and cycle performance of a 0.4 M cell, which achieved more than 85% utilization of the theoretical capacity of 214.4 mAh with a CE of 98.8% and an average EE of 73.6% for 30 cycles for 43.6 h, indicating a similar trend between high and low concentrations that is also expected to be related to higher concentrations. Hence, we also

https://doi.org/10.1021/acsenergylett.3c01293
ACS Energy Lett. 2023, 8, 3702−3709

conducted tests with higher concentration of the negolyte, which was paired with different amounts of the posolyte to estimate the stability of the negolyte. With this configuration, we can successfully demonstrate the capability for high-concentration operation of 0.8 M $K_3[Mn(CN)_6]$, attaining over 85% utilization of the theoretical capacity at a relatively high current density of 100 mA cm^{-2} for 1,000 cycles (Figure 3c and Supplementary Figure 5), while maintaining a CE of above 99%. This result underscores the promising potential of high-concentration operations employing the $[Mn(CN)_6]^{4-/3-}$ redox reaction.

In situ Raman spectroscopy revealed the efficient conversion of $[Mn(CN)_6]^{3-}$ and $[Mn(CN)_6]^{4-}$ during the charging and discharging processes, as shown in Figure 3d. The Raman-active CN stretch of $Mn(CN)_6$ ligands (v_1 and v_3 modes, see Supplementary Figure 6) and free cyanide ligands (CN^-) from the NaCN electrolyte can be observed in the range of 1900−2200 cm^{-1}. The v_1 and v_3 modes of $[Mn^{II}(CN)_6]^{4-}$ are detected at 2082 and 2066 cm^{-1}, respectively. For $[Mn^{III}(CN)_6]^{3-}$, the v_1 and v_3 values overlap at 2129 cm^{-1}, leading to a higher intensity compared with the peaks of Mn(I) and Mn(II). The CN stretch of free cyanide ligands (CN^-) was assigned to the frequency 2079 cm^{-1}, which coincided with the v_1 mode of $[Mn^{II}(CN)_6]^{4-}$ (2082 cm^{-1}) and was difficult to distinguish at the high state of charge (see also Supplementary Figure 6).[57] During charging of the flow cell, the peak intensity of the CN stretch of $[Mn^{III}(CN)_6]^{3-}$ (2129 cm^{-1}) decreased and completely disappeared at 1 V. In addition, the intensity of the $[Mn^{II}(CN)_6]^{4-}$ peaks (2066 and 2082 cm^{-1}) gradually increased, as demonstrated in the contour diagram of the Raman spectra in Figure 3d. The peak recovered its initial state reversibly after the discharging process.

Two-Electron Reaction. We also conducted full-cell tests using both $[Mn^{I}(CN)_6]^{5-}/[Mn^{II}(CN)_6]^{4-}$ and $[Mn^{II}(CN)_6]^{4-}/[Mn^{III}(CN)_6]^{3-}$ redox reactions for a negolyte. Although previous reports have not investigated the use of aqueous-based Mn(I)/Mn(II) redox reactions, we demonstrated that it is indeed feasible to operate rechargeable batteries using the Mn(I) oxidation state. A long cycle test of 0.1 M $K_3[Mn(CN)]_6$ cell at ±30 mA cm^{-2}, as shown in Figure 4a and Supplementary Figure 7, shows that it maintained an average 99.4% CE and 70.1% EE with 87% of its theoretical capacity for 178.0 h. In particular, CEs higher than 99% suggest that the redox reactions from Mn(III) to Mn(I) are reversibly repeated in the flow battery system. The reversible oxidation change of the $Mn(CN)_6$ ions during the two-electron reaction can also be verified through *in situ* Raman observations of the negolyte. Figure 4b presents the Raman spectrum of the negolyte side during one-cycle operation from 0.3 to 1.65 V. The CN-stretch peak positions of the $[Mn^{I}(CN)_6]^{5-}$ state are 1957 and 2024 cm^{-1}, which are v_3 and v_1 stretch modes, respectively. The gray shaded region of the right panel in Figure 4b represents the region of the $[Mn^{I}(CN)_6]^{5-}/[Mn^{II}(CN)_6]^{4-}$ redox reaction, showing that the $[Mn^{I}(CN)_6]^{5-}$ peaks (1957 and 2024 cm^{-1}) appear above 1.45 V during the charging process, whereas the intensity of the $[Mn^{II}(CN)_6]^{4-}$ peaks (2066 and 2082 cm^{-1}) tends to disappear. In the discharging region between 1.65 and 0.8 V, the $[Mn^{I}(CN)_6]^{5-}$ peaks decrease gradually, and the $[Mn^{II}(CN)_6]^{4-}$ peaks start to appear. The dotted box in the left panel in Figure 4b shows the magnified $[Mn^{I}(CN)_6]^{5-}$ peaks (1957 cm^{-1}), enabling elucidation of the variation of the Mn(I) state. Consequently, the $[Mn^{II}(CN)_6]^{4-}/[Mn^{III}(CN)_6]^{3-}$ redox reactions below 0.8 V reversibly cycle well, corresponding to Figure 3d. The contour diagrams corresponding to the Raman spectrum clearly validate the changes in intensity during cell operation.

In accordance with the results of our full-cell experiment, the oxidation state of Mn in hexacyanometalates undergoes effective conversion during repeated cyclic processes. However, the low solubility of $[Mn^{I}(CN)_6]^{5-}$ compounds, which are formed by the electrochemical reaction, limits their dissolution in the aqueous media to 0.016 M (K_{sp} = 2.1 × 10^{-11}).[46] As shown in Supplementary Figure 8, the limited solubility of $[Mn^{I}(CN)_6]^{5-}$ compounds results in a suspension above 1.6 V, while the precipitated compound is reversibly dissolved again during the discharging process. The *in situ* Raman spectra in Supplementary Figure 9 show the intensity variation of OH stretching, implying the precipitation and redissolution of Mn(I) compounds. The Raman peak intensity of OH stretching in H_2O tends to decrease as the solution concentration decreases.[58] In the Mn(I)/Mn(II) redox region in Supplementary Figure 9b, the intensity decreases, suggesting that the Mn(I) compound precipitated, and the solution concentration decreased. However, the intensity returned to the initial state after the discharging the cell, indicating the complete dissolution of the precipitated compound. In contrast, in the full-cell of the one-electron reaction, which does not accompany precipitation during cell operation, the intensity of OH stretching was maintained during the entire charge−discharge process (Supplementary Figure 9a). This trend can also be observed in the charging−discharging (Figure 4c) and dq/dV plots (Figure 4d) of some cycles, corresponding to Figure 4c. The region of the charging curve where the plateau shape begins to change in Figure 4c and the sharp peak appears in the dq/dV plot in Figure 4d (gray region) is considered the point at which hexacyanochromate-(I) salts begin to precipitate as the concentration of Mn(I) compounds in the solution exceeds its solubility limit. The presence of multiple voltage plateaus in the discharge profile of Figure 4c is also related to the oxidation process of precipitated Mn(I) salts. These plateaus arise from the coexistence of precipitated $Mn^{I}(s)$, $Mn^{I}(aq)$, and $Mn^{II}(aq)$ compounds, potentially leading to the formation of intermediate phases. These intermediate phases could occur due to the varying solubility and electrochemical behaviors of the different states, occurring at different reaction plateaus in the voltage profile. This observation underscores the complexity of the Mn(I)/Mn(II) redox process in the $Mn(CN)_6$ system, which involves both soluble and precipitated species.

We observed that the starting voltage of the abnormal plateau during the charging process decreased as the number of cycles increased at the 3rd, 10th, and 100th cycles. This is attributed to the precipitation of the Mn(I) compound occurring earlier due to the transportation of K^+ cations from the posolyte to the negolyte. The solubility of hexacyanomanganate(I) compounds is known to vary depending on the types of countercations, with $Na_5[Mn^{I}(CN)_6]$ having higher solubility as 0.899 M (K_{sp} = 0.53) than $K_5[Mn(CN)_6]$.[46] Despite the extremely low solubility of $K_5[Mn(CN)_6]$, the $[Mn^{I}(CN)_6]^{5-}/[Mn^{II}(CN)_6]^{4}$ redox reaction was well repeated due to the Na^+ cations provided by the NaCN supporting electrolyte. This study has successfully demonstrated the implementation of the multielectron reaction of manganese in an aqueous solution, which is

https://doi.org/10.1021/acsenergylett.3c01293
ACS Energy Lett. 2023, 8, 3702−3709

unprecedented due to the unstable redox couples in aqueous solutions. Although $Mn(CN)_6$ is capable of undergoing an acceptable two-electron reaction, the solubility of Mn(I) has been a significant concern. However, this study is the first to apply redox-flow-battery systems using Mn(I) in a solution state. Furthermore, we propose that the solubility of Mn(I) compounds can be sufficiently improved in future work by using various countercations and supporting electrolytes, as demonstrated in similar compounds like hexacyanoferrates.[59,60]

Our findings highlight the beneficial impact of supporting electrolytes in mitigating ligand exchanges at lower reaction potentials under hydrogen evolution reactions. By harnessing these advantages, the proposed $[Mn(CN)_6]^{5-/4-/3-}$ negolyte can operate over prolonged cycles. However, it is crucial to pay attention to safety issues related to free cyanides (HCN and CN^-). Gaseous HCN poses a significant inhalation risk, and its concentration increases at low pH. In our system, most of the free cyanides in the present system exist in the form of CN^- in the electrolyte solution because the operating pH of the electrolytes is between 13 and 14. Nevertheless, extreme precautions must be taken to ensure safe handling of cyanide ions and compliance with safety regulations in RFB applications.

In conclusion, we have developed manganese-based hexacyanometalate compounds for a negolyte in aqueous RFBs, allowing for the efficient use of multielectron reactions of manganese and overcoming the previous challenges of instability of manganese redox couples in aqueous environments. Moreover, the facile reversible change of Mn oxidation states from I to III in a full-cell configuration was effectively demonstrated using *in situ* Raman spectroscopy. The prototype full-cell using the two-electron $Mn(CN)_6$ redox reaction exhibits a stable lifetime of up to 100 cycles using 0.1 M negolyte. Although the solubility of the Mn(I) compound remains a challenge, this study demonstrates the potential of using Mn(I) in solution in aqueous rechargeable batteries. Our findings offer new opportunities for the exploration and development of low-cost manganese-based redox systems and represent a significant breakthrough in the field of redox chemistry toward the design of higher-energy-density RFBs.

■ ASSOCIATED CONTENT

Supporting Information

The Supporting Information is available free of charge at https://pubs.acs.org/doi/10.1021/acsenergylett.3c01293.

Experimental details and additional figures and tables as described in the text (PDF)

■ AUTHOR INFORMATION

Corresponding Author

Hyun-Wook Lee − *School of Energy and Chemical Engineering, Ulsan National Institute of Science and Technology (UNIST), Ulsan 44919, Republic of Korea;* orcid.org/0000-0001-9074-1619; Email: hyunwooklee@unist.ac.kr

Authors

Ji-Eun Jang − *School of Energy and Chemical Engineering, Ulsan National Institute of Science and Technology (UNIST), Ulsan 44919, Republic of Korea*

S. Jayasubramaniyan − *School of Energy and Chemical Engineering, Ulsan National Institute of Science and Technology (UNIST), Ulsan 44919, Republic of Korea*

Seok Woo Lee − *School of Electrical and Electronic Engineering, Nanyang Technological University, Singapore 639798, Singapore;* orcid.org/0000-0003-2459-7174

Complete contact information is available at: https://pubs.acs.org/10.1021/acsenergylett.3c01293

Notes

The authors declare no competing financial interest.

■ ACKNOWLEDGMENTS

This work was supported by the 2023 Research Fund (1.230040.01) of UNIST, Individual Basic Science & Engineering Research Program through National Research Foundation of Korea (NRF) funded by the Ministry of Science and ICT (RS-2023-00208929), and the Ministry of Trade, Industry & Energy/Korea Institute of Energy Technology Evaluation and Planning (MOTIE/KETEP) (20224000000390). S.W.L. acknowledges the support by the National Research Foundation, Prime Minister's Office, Singapore under its NRF-ANR Joint Programme (NRF2019-NRF-ANR052 KineHarvest). This study contains the results obtained by using the equipment of UNIST Central Research Facilities (UCRF).

■ REFERENCES

(1) Yang, Z.; Zhang, J.; Kintner-Meyer, M. C. W.; Lu, X.; Choi, D.; Lemmon, J. P.; Liu, J. Electrochemical Energy Storage for Green Grid. *Chem. Rev.* **2011**, *111* (5), 3577−3613.

(2) Chu, S.; Majumdar, A. Opportunities and Challenges for a Sustainable Energy Future. *Nature* **2012**, *488* (7411), 294−303.

(3) Bullich-Massague, E.; Cifuentes-Garcia, F.-J.; Glenny-Crende, I.; Cheah-Mane, M.; Aragues-Penalba, M.; Diaz-Gonzalez, F.; Gomis-Bellmunt, O. A Review of Energy Storage Technologies for Large Scale Photovoltaic Power Plants. *Appl. Energy* **2020**, *274*, 115213.

(4) Wang, W.; Luo, Q.; Li, B.; Wei, X.; Li, L.; Yang, Z. Recent Progress in Redox Flow Battery Research and Development. *Adv. Funct. Mater.* **2013**, *23* (8), 970−986.

(5) Park, M.; Ryu, J.; Wang, W.; Cho, J. Material Design and Engineering of Next-Generation Flow-Battery Technologies. *Nat. Rev. Mater.* **2017**, *2* (1), 16080.

(6) Soloveichik, G. L. Flow Batteries: Current Status and Trends. *Chem. Rev.* **2015**, *115* (20), 11533−11558.

(7) Leung, P.; Li, X.; Ponce De León, C.; Berlouis, L.; Low, C. T. J.; Walsh, F. C. Progress in Redox Flow Batteries, Remaining Challenges and Their Applications in Energy Storage. *RSC Adv.* **2012**, *2* (27), 10125−10156.

(8) Zhang, L.; Feng, R.; Wang, W.; Yu, G. Emerging Chemistries and Molecular Designs for Flow Batteries. *Nat. Rev. Chem.* **2022**, *6*, 524−543.

(9) Thaller, L. Redox Flow Cell Energy Storage Systems, *Terrestrial Energy Systems Conference*, 1979. DOI: 10.2514/6.1979-989.

(10) Skyllas-Kazacos, M.; Grossmith, F. Efficient Vanadium Redox Flow Cell. *J. Electrochem. Soc.* **1987**, *134* (12), 2950−2953.

(11) Xiong, F.; Zhou, D.; Xie, Z.; Chen, Y. A Study of the Ce3+/Ce4+ Redox Couple in Sulfamic Acid for Redox Battery Application. *Appl. Energy* **2012**, *99*, 291−296.

(12) Cheng, Y.; Xi, X.; Li, D.; Li, X.; Lai, Q.; Zhang, H. Performance and Potential Problems of High Power Density Zinc-Nickel Single Flow Batteries. *RSC Adv.* **2015**, *5* (3), 1772−1776.

(13) Wu, M. C.; Zhao, T. S.; Jiang, H. R.; Zeng, Y. K.; Ren, Y. X. High-Performance Zinc Bromine Flow Battery via Improved Design of Electrolyte and Electrode. *J. Power Sources* **2017**, *355*, 62−68.

(14) Xie, C.; Duan, Y.; Xu, W.; Zhang, H.; Li, X. A Low-Cost Neutral Zinc-Iron Flow Battery with High Energy Density for Stationary Energy Storage. *Angew. Chemie - Int. Ed.* **2017**, *56* (47), 14953−14957.
(15) Huskinson, B.; Marshak, M. P.; Suh, C.; Er, S.; Gerhardt, M. R.; Galvin, C. J.; Chen, X.; Aspuru-Guzik, A.; Gordon, R. G.; Aziz, M. J. A Metal Free Organic- Inorganic Aqueous Flow Battery. *Nature* **2014**, *505*, 195−198.
(16) Lin, K.; Chen, Q.; Gerhardt, M. R.; Tong, L.; Kim, S. B.; Eisenach, L.; Valle, A. W.; Hardee, D.; Gordon, R. G.; Aziz, M. J.; Marshak, M. P. Alkaline Quinone Flow Battery. *Science* **2015**, *349* (6255), 1529−1532.
(17) Janoschka, T.; Martin, N.; Martin, U.; Friebe, C.; Morgenstern, S.; Hiller, H.; Hager, M. D.; Schubert, U. S. An Aqueous, Polymer-Based Redox-Flow Battery Using Non-Corrosive, Safe, and Low-Cost Materials. *Nature* **2015**, *527* (7576), 78−81.
(18) Li, X.; Gao, P.; Lai, Y. Y.; Bazak, J. D.; Hollas, A.; Lin, H. Y.; Murugesan, V.; Zhang, S.; Cheng, C. F.; Tung, W. Y.; Lai, Y. T.; Feng, R.; Wang, J.; Wang, C. L.; Wang, W.; Zhu, Y. Symmetry-Breaking Design of an Organic Iron Complex Catholyte for a Long Cyclability Aqueous Organic Redox Flow Battery. *Nat. Energy* **2021**, *6* (9), 873−881.
(19) Feng, R.; Zhang, X.; Murugesan, V.; Hollas, A.; Chen, Y.; Shao, Y.; Walter, E.; Wellala, N. P. N.; Yan, L.; Rosso, K. M.; Wang, W. Reversible Ketone Hydrogenation and Dehydrogenation for Aqueous Organic Redox Flow Batteries. *Science* **2021**, *372* (6544), 836−840.
(20) da Silva Lima, L.; Quartier, M.; Buchmayr, A.; Sanjuan-Delmás, D.; Laget, H.; Corbisier, D.; Mertens, J.; Dewulf, J. Life Cycle Assessment of Lithium-Ion Batteries and Vanadium Redox Flow Batteries-Based Renewable Energy Storage Systems. *Sustain. Energy Technol. Assessments* **2021**, *46*, 101286.
(21) Jiang, H. R.; Sun, J.; Wei, L.; Wu, M. C.; Shyy, W.; Zhao, T. S. A High Power Density and Long Cycle Life Vanadium Redox Flow Battery. *Energy Storage Mater.* **2020**, *24*, 529−540.
(22) Jang, J.-E.; Kim, R.-a.; Jayasubramaniyan, S.; Lee, C.; Choi, J.; Lee, Y.; Kang, S.; Ryu, J.; Lee, S. W.; Cho, J.; Lee, D. W.; Song, H.-K.; Choe, W.; Seo, D.-H.; Lee, H.-W. Full-Hexacyanometallate Aqueous Redox Flow Batteries Exceeding 1.5 V in an Aqueous Solution. *Adv. Energy Mater.* **2023**, 230707.
(23) Li, H.; Zhang, W.; Sun, K.; Guo, J.; Yuan, K.; Fu, J.; Zhang, T.; Zhang, X.; Long, H.; Zhang, Z.; Lai, Y.; Sun, H. Manganese-Based Materials for Rechargeable Batteries beyond Lithium-Ion. *Adv. Energy Mater.* **2021**, *11*, 2100867.
(24) Naresh, R. p.; Mariyappan, K.; Dixon, D.; Ulaganathan, M.; Ragupathy, P. Investigations on New Electrolyte Composition and Modified Membrane for High Voltage Zinc-Manganese Hybrid Redox Flow Batteries. *Batter. Supercaps* **2021**, *4* (9), 1464−1472.
(25) Wu, J.; Yang, J.; Leong, Z. Y.; Zhang, F.; Deng, H.; Ouyang, G. F.; Yu, J. A Method to Inhibit Disproportionation of Mn3+for Low-Cost Mn-Fe All-Flow Battery. *ACS Appl. Energy Mater.* **2022**, *5* (12), 14646−14651.
(26) Xue, F. Q.; Wang, Y. L.; Wang, W. H.; Wang, X. D. Investigation on the Electrode Process of the Mn(II)/Mn(III) Couple in Redox Flow Battery. *Electrochim. Acta* **2008**, *53* (22), 6636−6642.
(27) Soldatova, A. V.; Romano, C. A.; Tao, L.; Stich, T. A.; Casey, W. H.; Britt, R. D.; Tebo, B. M.; Spiro, T. G. Mn(II) Oxidation by the Multicopper Oxidase Complex Mnx: A Coordinated Two-Stage Mn(II)/(III) and Mn(III)/(IV) Mechanism. *J. Am. Chem. Soc.* **2017**, *139*, 11381−11391.
(28) Chen, W.; Li, G.; Pei, A.; Li, Y.; Liao, L.; Wang, H.; Wan, J.; Liang, Z.; Chen, G.; Zhang, H.; Wang, J.; Cui, Y. A Manganese-Hydrogen Battery with Potential for Grid-Scale Energy Storage. *Nat. Energy* **2018**, *3*, 428−435.
(29) Li, G.; Chen, W.; Zhang, H.; Gong, Y.; Shi, F.; Wang, J.; Zhang, R.; Chen, G.; Jin, Y.; Wu, T.; Tang, Z.; Cui, Y. Membrane-Free Zn/MnO2 Flow Battery for Large-Scale Energy Storage. *Adv. Energy Mater.* **2020**, *10* (9), 1902085.
(30) Qiao, L.; Xie, C.; Nan, M.; Zhang, H.; Ma, X.; Li, X. Highly Stable Titanium-Manganese Single Flow Batteries for Stationary Energy Storage. *J. Mater. Chem. A* **2021**, *9* (21), 12606−12611.
(31) Lei, J.; Yao, Y.; Huang, Y.; Lu, Y. C. A Highly Reversible Low-Cost Aqueous Sulfur-Manganese Redox Flow Battery. *ACS Energy Lett.* **2023**, *8* (1), 429−435.
(32) Chao, D.; Zhou, W.; Ye, C.; Zhang, Q.; Chen, Y.; Gu, L.; Davey, K.; Qiao, S. Z. An Electrolytic Zn-MnO2 Battery for High-Voltage and Scalable Energy Storage. *Angew. Chemie - Int. Ed.* **2019**, *58* (23), 7823−7828.
(33) Xie, C.; Li, T.; Deng, C.; Song, Y.; Zhang, H.; Li, X. A Highly Reversible Neutral Zinc/Manganese Battery for Stationary Energy Storage. *Energy Environ. Sci.* **2020**, *13* (1), 135−143.
(34) Lei, J.; Yao, Y.; Wang, Z.; Lu, Y. C. Towards High-Areal-Capacity Aqueous Zinc-Manganese Batteries: Promoting MnO2dis-solution by Redox Mediators. *Energy Environ. Sci.* **2021**, *14* (8), 4418−4426.
(35) Schmucker, M.; Gully, T. A.; Schmidt, A.; Schmidt, B.; Bromberger, K.; Disch, J.; Butschke, B.; Burgenmeister, B.; Sonnenberg, K.; Riedel, S.; Krossing, I. Investigations toward a Non-Aqueous Hybrid Redox-Flow Battery with a Manganese-Based Anolyte and Catholyte. *Adv. Energy Mater.* **2021**, *11* (24), 2101261.
(36) Wang, M.; Zheng, X.; Zhang, X.; Chao, D.; Qiao, S.; Alshareef, H. N.; Cui, Y.; Chen, W. Opportunities of Aqueous Manganese-Based Batteries with Deposition and Stripping Chemistry. *Adv. Energy Mater.* **2021**, *11* (5), 2002904.
(37) Yang, Q.; Qu, X.; Cui, H.; He, X.; Shao, Y.; Zhang, Y.; Guo, X.; Chen, A.; Chen, Z.; Zhang, R.; Kong, D.; Shi, Z.; Liu, J.; Qiu, J. Rechargeable Aqueous Mn-Metal Battery Enabled by Inorganic - Angewandte. *Angew. Chem., Int. Ed.* **2022**, *61*, e202206471.
(38) Dong, Y.-R.; Kaku, H.; Hanafusa, K.; Moriuchi, K.; Shigematsu, T. A Novel Titanium/Manganese Redox Flow Battery. *ECS Trans.* **2015**, *69* (18), 59.
(39) Reynard, D.; Maye, S.; Peljo, P.; Chanda, V.; Girault, H. H.; et al. Vanadium - Manganese Redox Flow Battery : Study of Mn III Disproportionation in the Presence of Other Metallic Ions. *Chem. - Eur. J.* **2020**, *26*, 7250−7257.
(40) Zhang, H.; Wang, Z. Geochemical Stability of Dissolved Mn(III) in the Presence of Pyrophosphate as a Model Ligand: Complexation and Disproportionation. *Environ. Sci. Technol.* **2019**, *53*, 5768−5777.
(41) Robb, B. H.; Farrell, J. M.; Marshak, M. P. Chelated Chromium Electrolyte Enabling High-Voltage Aqueous Flow Batteries. *Joule* **2019**, *3* (10), 2503−2512.
(42) Yu, X.; Song, Y.; Tang, A. Tailoring Manganese Coordination Environment for a Highly Reversible Zinc-Manganese Flow Battery. *J. Power Sources* **2021**, *507*, 230295.
(43) Sleightholme, A. E. S.; Shinkle, A. A.; Liu, Q.; Li, Y.; Monroe, C. W.; Thompson, L. T. Non-Aqueous Manganese Acetylacetonate Electrolyte for Redox Flow Batteries. *J. Power Sources* **2011**, *196* (2011), 5742−5745.
(44) Sharpe, A. G. In *The Chemistry of Cyano Complexes of the Transition Metals*; Maltlis, P. M., Stone, F. G. A., Eds.; Academic Press: 1976; pp 75−88.
(45) Meyer, J. Zur Kenntnis Des Dreiwertigen Mangans 1. *Z. fur Anorg. Allg. Chem.* **1913**, *81* (1), 385−405.
(46) Treadwell, W. D.; Raths, W. E. Zur Kenntnis von Natrium-Und Kaliumhexacyanomanganat (I). *Helv. Chim. Acta* **1952**, *35* (282), 2259−2275.
(47) Singh, V.; Kim, S.; Kang, J.; Byon, H. R. Aqueous Organic Redox Flow Batteries. *Nano Res.* **2019**, *12* (9), 1988−2001.
(48) Yao, Y.; Lei, J.; Shi, Y.; Ai, F.; Lu, Y. C. Assessment Methods and Performance Metrics for Redox Flow Batteries. *Nat. Energy* **2021**, *6*, 582−588.
(49) Huang, R.; Liu, S.; He, Z.; Zhu, W.; Ye, G.; Su, Y.; Deng, W.; Wang, J. Electron-Deficient Sites for Improving V 2 + /V 3 + Redox Kinetics in Vanadium Redox Flow Batteries. *Adv. Funct. Mater.* **2022**, *32*, 2111661.

https://doi.org/10.1021/acsenergylett.3c01293
ACS Energy Lett. 2023, 8, 3702−3709

(50) Treadwell, W. D.; Raths, W. E. Uber Die Darstellung von Cyanomanganat(I) Durch Reduktion Mit Unedeln Metallen. *Helv. Chim. Acta* **1952**, *35* (7), 2275−2280.
(51) Esswein, A. J. et al. Aqueous Redox Flow Batteries Featuring Improved Cell Design Characteristics, U.S. Patent, Pub. No. US 2014/0030573 A1, 2014.
(52) Goeltz, et al. Aqueous Redox Flow Batteries Comprising Metal Ligand Coordination Compounds, U.S. Patent, Pub. No. US 2017/0352905 A1, 2017.
(53) Lee, H. W.; Wang, R. Y.; Pasta, M.; Lee, S. W.; Liu, N.; Cui, Y. Manganese Hexacyanomanganate Open Framework as a High-Capacity Positive Electrode Material for Sodium-Ion Batteries. *Nat. Commun.* **2014**, *5*, 5280.
(54) Hurlbutt, K.; Giustino, F.; Volonakis, G.; Pasta, M. Origin of the High Specific Capacity in Sodium Manganese Hexacyanomanganate. *Chem. Mater.* **2022**, *34*, 4336−4343.
(55) Choi, A.; Kim, T.; Kim, M. H.; Lee, S. W.; Jung, Y. H.; Lee, H. W. Mitigating Jahn-Teller Effects by Fast Electrode Kinetics Inducing Charge Redistribution. *Adv. Funct. Mater.* **2022**, *32* (19), 2111901.
(56) Nicholson, R. S. Theory and Application of Cyclic Voltammetry for Measurement of Electrode Reaction Kinetics. *Anal. Chem.* **1965**, *37* (11), 1351−1355.
(57) Griffith, W. P.; Turner, G. T. Raman Spectra and Vibrational Assignments of Hexacyano-Complexes. *J.Chem.Soc.(A).* **1970**, 858−862.
(58) Patra, A.; Roy, S.; Saha, S.; Palit, D. K.; Mondal, J. A. Observation of Extremely Weakly Interacting OH (∼3600 Cm-1) in the Vicinity of High Charge Density Metal Ions (Mz+ z = 1, 2, 3): A Structural Heterogeneity in the Extended Hydration Shell. *J. Phys. Chem. C* **2020**, *124* (5), 3028−3036.
(59) Luo, J.; Sam, A.; Hu, B.; DeBruler, C.; Wei, X.; Wang, W.; Liu, T. L. Unraveling PH Dependent Cycling Stability of Ferricyanide/Ferrocyanide in Redox Flow Batteries. *Nano Energy* **2017**, *42*, 215−221.
(60) Luo, J.; Hu, B.; Debruler, C.; Bi, Y.; Zhao, Y.; Yuan, B.; Hu, M.; Wu, W.; Liu, T. L. Unprecedented Capacity and Stability of Ammonium Ferrocyanide Catholyte in PH Neutral Aqueous Redox Flow Batteries. *Joule* **2019**, *3* (1), 149−163.

https://doi.org/10.1021/acsenergylett.3c01293
ACS Energy Lett. 2023, 8, 3702−3709